



## **Azimuthal Anisotropy Investigations for P and S Waves: A Physical Modelling Experiment**

*Khaled Al Dulaijan, Gary F. Margrave, and Joe Wong*  
CREWES

### **Summary**

A two-layer model was built using vertically laminated Phenolic overlain by Plexiglas to represent a fractured reservoir overlaid by an isotropic overburden. The first dataset was acquired over that 2-layer model and consist of three 9-component common-receivers. P-wave first-arrival times were analyzed on all three gathers and fracture orientation was predicted. An Alford rotation was applied to the four horizontal components and successfully minimized energy on components other than those two that are related to the fast S wave and slow S wave. However, the angle between natural and acquisition coordinate systems was not predicted correctly. One possible reason could be the contact between the two media. Therefore, another dataset was acquired using a single Phenolic layer. Alford rotation was applied and the angle between natural and acquisition coordinate system was predicted correctly. That dataset was used too to measure the stiffness coefficients tensor using group velocity data.

### **Introduction**

In the physical modeling laboratory, a fractured reservoir and isotropic overburden can be represented by two layers: one anisotropic and one isotropic. Because azimuthal anisotropy is of interest to us, we want to acquire gathers of common offset and varying azimuthal angles. In such a way, fracture orientation can be predicted from azimuthal analysis of P-wave first arrival times. Also, it can be predicted by S-wave splitting because fast S wave polarization direction indicates directly the orientation of fractures (Winterstein, 1994). Regularly, a four-component horizontal rotation (i.e. Alford rotation) is needed to separate the fast S wave from the slow S wave. Azimuthal common-offset receiver gathers have wide range of azimuth angles but limited range of angle of incidence. Shots are distributed along a circle covering 360o azimuth. Therefore, they are ideal for Horizontally-Transverse Isotropy (HTI) media. In this study, common azimuth shot gathers were also collected and analyzed. Such gathers are ideal for Vertically-Transverse Isotropy (VTI) media. Two data sets were acquired over different models for this report:

1. Three circular common-receiver gathers with radii equal to 250 m, 500 m and 1000 m were acquired over a 2-layer model. In that dataset, a 3-C receiver and a 3-C source yield produce 9-C receiver gathers.

2. One circular gather, which has a 200 m radius, and two linear gathers with 0o and 90o azimuths were acquired over the anisotropic medium. In that dataset, a 3-C receiver and a 2-C horizontal source resulted in 6-C shot gathers.

Alford rotation analysis was the motivation for acquiring the second dataset because results of the first dataset for the rotational analysis were not as predicted from the physical model.

### **P-wave first-arrival times analysis**

Three common-receiver gathers at  $r = 250$  m, 500 m and 1000 m are shown in Figures 1-3. Each gather ( $v_{ij}$ ) is composed of 9 components. The first subscript of  $v$  denotes the receiver component, while the

second subscript denotes the source component. The x-, y-, and z-components are labeled by the numbers 1, 2, and 3 respectively. For example,  $v_{31}$  was acquired with a vertical receiver due to a source along the x-axis.

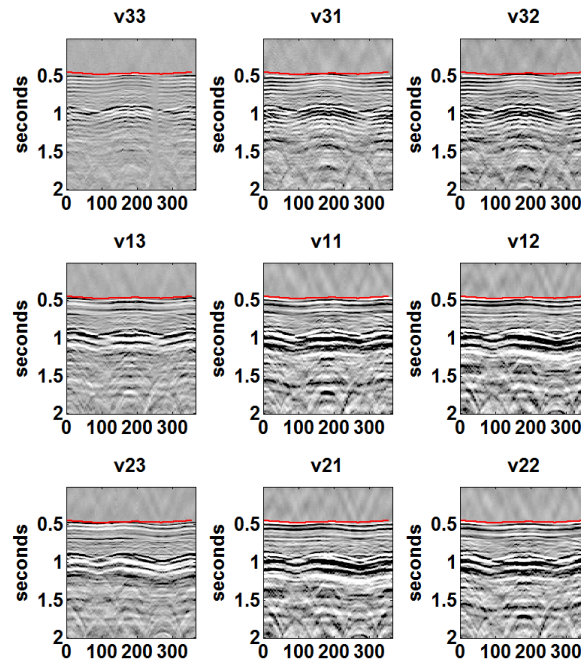


FIG. 1. 9-C receiver gather with  $r = 1000$  m. P-wave first arrival times are indicated by red. The horizontal axis is the azimuth angles which go from  $0^\circ$  to  $360^\circ$  with a  $4^\circ$  increment.

The common-receiver gathers in Figures 1 is plotted with the same amplitude range. Azimuth varies from  $0^\circ$  to  $360^\circ$  with an increment of  $4^\circ$  for the 1<sup>st</sup> to the 90<sup>th</sup> trace. First arrival times were picked on first onset and indicated by red. The 250-m and 500-m common-receiver gathers show nearly constant first-arrival times with increasing azimuth angle (not shown here). The 1000-m common-receiver gather show a sinusoidal variation of first arrival times with increasing azimuth angle. The acquisition layout suggests that components  $v_{11}$  of the three gathers are acquired with horizontal receivers and sources whose polarization directions are along the x-axis (or parallel to fracture plane). Similarly,  $v_{22}$  components have transducer polarization perpendicular to fracture plane.

In isotropic media, P-wave first-arrival times are constant for the same offset and different azimuths. Each common-receiver gather has a constant offset. Figure 1 shows first-arrival times that are variant with azimuth angle and look like a sinusoidal function. Early first arrivals are at  $0^\circ$ ,  $180^\circ$ , and  $360^\circ$ . Those angles define the fast P-wave direction which is parallel to the fracture plane. This result is in agreement with the physical model where fracture plane within the Phenolic is along **x**-axis. If plotted azimuthally in a polar view, sinusoidal first-arrival times appear as an ellipse. The minor axis of the ellipse indicates early first-arrival times, while the major axis indicates late first-arrival times. Therefore, the minor axis indicates the fracture plane (Al Dulaijan et al., 2012).

For each common-receiver gather, first-arrival times are plotted azimuthally in a polar view. Then by least-squares fitting, an ellipse is fitted. Figures 2 show elliptical fitting of first-arrival. The minor axis for the third gather is  $1^\circ$ . The minor axes indicate the fracture plane which is supposed to be  $0^\circ$  according to the physical model. The first and second common-receiver gathers have a smaller offset than the third gather, and therefore are more sensitive to acquisition inaccuracies.

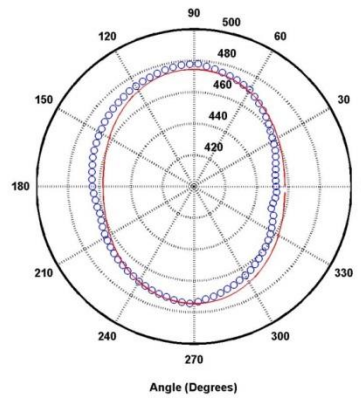


FIG. 2. Elliptical fitting of first-arrival times for the third receiver gather ( $r = 1,000$  m). The minor axis is at  $1^0$ .

### S-wave splitting: Alford rotation

In the HTI media, the P wave is fastest along the fracture planes, slowest perpendicular to fracture planes, somewhere in between in other direction. On the other hand, S wave has to split into two phases; a phenomena known as S-wave splitting, S-wave birefringence, or S-wave double-refraction. Polarizations of the two S waves are determined by anisotropy axis of symmetry. The fast S is polarized along the fracture planes and slow S is perpendicular to the fracture planes. Beside the anisotropy axis of symmetry, the velocity of S wave is controlled also by the angle of incidence and the azimuth of propagation. The two S waves travel at different velocities (within the Phenolic) and are recorded at different times. The delay in time is proportionally related to the degree of S-wave anisotropy and thickness of the anisotropic medium (Crampin, 1981).

For all three common-receiver gathers, horizontal components of receivers and sources were aligned along  $x$ - or  $y$ -axis. In other words, they were aligned either parallel to fracture plane or normal to the fracture plane. In such a way, S wave is fast along  $y$ -axis and slow along  $x$ -axis. In other directions, S wave undergoes S-wave splitting and repolarizes along fast and slow directions. Fast S wave should mostly be recorded by  $v_{11}$  and slow S wave by  $v_{22}$ . Energy on  $v_{12}$  and  $v_{21}$  should be minimal. This was not the case in our experiment! That suggests an error in the polarization direction of the horizontal transducers.

An Alford 4-component rotation (Alford, 1986) can be used to statistically rotate horizontal components ( $\mathbf{V}$ ) recorded in acquisition recorded system into anisotropy natural coordinate system ( $\mathbf{U}$ ). The rotation angle ( $\theta$ ) is found by scanning different angle values, and then selecting the angle that minimizes  $u_{12}$  and/or  $u_{21}$ . For each common-receive gather, angles were scanned within a time window to determine the rotation angle ( $\theta$ ) and Alford rotation was applied. All three gathers acquired over the 2-layer model have rotation angles around  $45^\circ$ . Ideally, Alford rotation is not needed for this dataset because the acquisition and natural system coordinate are identical. However, this was not the case. One possible reason may be the contact between the Plexiglas and the Phenolic or lack thereof. Therefore, the second dataset was acquired over the Phenolic medium only. The second dataset consists of one circular gather which has 200 m radius and two linear gathers with  $0^\circ$  and  $90^\circ$  azimuths. Alford rotation was applied to the second dataset as well. Four horizontal components of the  $90^\circ$ -azimuth shot gather is shown before rotation on the left of Figure 3 and after rotation on the right of the same figure. Figure 4 shows the cross energy of different rotation angles. For this common-receiver gather, the rotation angle ( $\theta$ ) is  $0^\circ$ .

Using the second dataset, Alford rotation behavior is just as anticipated. The rotation angles are very small because acquisition coordinate system is similar to the natural coordinate system. The small angles are caused by small errors in acquisition. The results of Alford rotation for the second dataset are quite satisfying. They provide confidence in S-wave acquisition tools.

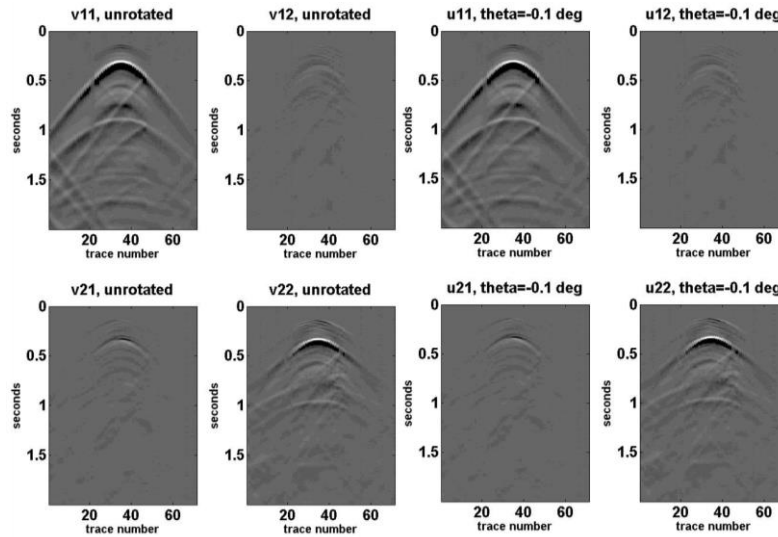


Fig. 3. 90°-azimuth shot gather acquired over the Phenolic layer: 4 Horizontal components before rotation (left) and after rotation (right).

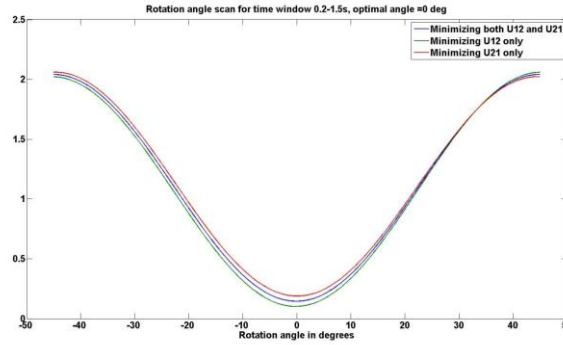


FIG. 4. 90°-azimuth shot gather: cross energy vs. rotation angle.

### Estimation of elastic stiffness coefficients

In anisotropic media, phase and group velocities are not equal. Group velocities at different angles of incidence ( $\Theta$ ) and azimuthal angles ( $\Phi$ ) can be easily measured in laboratory, as well in field. For orthorhombic media, Daley and Krebs (2006) have derived a relation between the P group velocity ( $V$ ) and the density-normalized stiffness coefficients ( $A_{ij}$ ):

$$\frac{1}{V^2(\vec{N})} \approx \frac{N_1^2}{A_{11}} + \frac{N_2^2}{A_{22}} + \frac{N_3^2}{A_{33}} - \frac{E_{23}N_2^2N_3^2}{A_{22}A_{33}} - \frac{E_{13}N_1^2N_3^2}{A_{11}A_{33}} - \frac{E_{12}N_1^2N_2^2}{A_{11}A_{22}}, \quad (1)$$

In the laboratory,  $\sqrt{A_{44}}$ ,  $\sqrt{A_{55}}$ , and  $\sqrt{A_{66}}$  were measured.  $\sqrt{A_{33}}$  was measured too, but was assumed unknown in the inversion in order to use it to validate the results. Five stiffness coefficients ( $A_{11}$ ,  $A_{22}$ ,  $A_{33}$ ,  $A_{12}$ ,  $A_{13}$ , and  $A_{23}$ ) are inverted for. For the inversion the second dataset is used. That dataset consists of 3 common-shot gathers: one circular that has 200 m radius; and two linear at 0° and 90° azimuths. First P-wave arrival times are picked and used to calculate P group velocities by dividing distance between source and receiver over the time. The circular gather has a wide range of azimuthal angles and a single angle of incidence that is approximately 24°. The line gathers have a single azimuthal angle 0° or 90°

and a wide range of incidence angles. Three measured coefficients and six inverted coefficients from the density-normalized stiffness coefficients of the Phenolic layer in ( $m^2/s^2$ ) are as follows:

$$A_{ij} = \begin{bmatrix} 1.3280e+07 & 1.0946e+07 & 4.9801e+06 & 0 & 0 & 0 \\ 1.0946e+07 & 8.7328e+06 & 6.2308e+06 & 0 & 0 & 0 \\ 4.9801e+06 & 6.2308e+06 & 1.1114e+07 & 0 & 0 & 0 \\ 0 & 0 & 0 & 2.1072e+06 & 0 & 0 \\ 0 & 0 & 0 & 0 & 2.4414e+06 & 0 \\ 0 & 0 & 0 & 0 & 0 & 3.1888e+06 \end{bmatrix} \quad (2)$$

$V_{11}$	$V_{22}$	$V_{33}$	$V_{23}$	$V_{13}$	$V_{12}$
3644.1	2955.1	3333.7	1451.6	1562.5	1785.7

Table 1. Body wave velocities ( $V_{ij}$ ) that propagates along  $x_r$ -axis and polarized along  $x_f$ -axis in (m/s).

## Conclusions

Table 1 summarizes body wave group velocities ( $V_{ij}$ ) in the Phenolic. Physical modeling is a valuable tool that can assist in the evaluation and development of practices for fracture characterization. This report has utilized physical modeling, and in summary:

- Fracture plane orientation was easily identified from the third common-receiver gather ( $r = 1000$  m) by P-wave first-arrival times. Elliptical fitting of P-wave first-arrival times was employed to identify the fracture plane orientation from the three common-receiver gather.
- An Alford rotation was applied to dataset that was acquired over 2-layer model to transform the data from acquisition system coordinate to natural system coordinate. Results of Alford analysis were not as anticipated and that was the motivation to acquire the second dataset.
- Alford rotational analysis was applied to the 2<sup>nd</sup> dataset. The results of Alford rotation for the 2<sup>nd</sup> dataset are quite satisfying because they provide confidence in S-wave acquisition tools.
- 2<sup>nd</sup> dataset was used to invert for the elastic stiffness coefficients of the Phenolic medium over which it was acquired.

## Acknowledgments

We thank the sponsors of CREWES for their support, and NSERC (Natural Science and Engineering Research Council of Canada) through the grant CRDPJ 379744-08.

## References

- Al Dulaijan, K., Owusu, J. C., & Weber, D. C., 2012, Azimuthal anisotropy analysis of walkaround vertical seismic profiling vertical seismic profiling: a case study from Saudi Arabia. *Geophysical Prospecting*, 60(6), 1082-1094.
- Alford, R. M., 1986, Shear data in the presence of azimuthal anisotropy: Dilley Texas, SEG Expanded Abstracts, SEG Annual Convention.
- Crampin, S., 1981, A review of wave motion in anisotropic and cracked elastic-media. *Wave motion*, 3(4), 343-391.
- Daley, P. F., and E. S. Krebs, 2006, Quasi-compressional group velocity approximation in a weakly anisotropic orthorhombic medium: *Journal of Seismic Exploration*, 14, 319-334.
- Mahmoudian, F., Margrave, G., Daley, P., Wong, J., and Henley, D., 2014, Estimation of elastic stiffness coefficients of an orthorhombic physical model using group velocity analysis on transmission data. *Geophysics*, 79, R27-R39.
- Winterstein, D., 1992, How shear-wave properties relate to rock fractures: Simple cases. *The Leading Edge*, 11(9), 21-28.